REPORT DOCUMENTATION PAGE

Form Approved
OMB No. 0704-0188

1. REPORT DATE *(DD-MM-YYYY)*	2. REPORT TYPE	3. DATES COVERED *(From - To)*
30-Sep-2008	REPRINT	

4. TITLE AND SUBTITLE
IMPROVED PHASE CHARACTERIZATION OF FAR-REGIONAL BODY WAVE ARRIVALS IN CENTRAL ASIA

5a. CONTRACT NUMBER
FA8718-06-C-0002

5b. GRANT NUMBER

5c. PROGRAM ELEMENT NUMBER
62601F

6. AUTHOR(S)
Aaron Ferris, Delaine Reiter, and Anastasia Stroujkova

5d. PROJECT NUMBER
1010

5e. TASK NUMBER
SM

5f. WORK UNIT NUMBER
A1

7. PERFORMING ORGANIZATION NAME(S) AND ADDRESS(ES)

Weston Geophysical Corporation
181 Bedford St., Suite 1
Lexington, MA 02420

8. PERFORMING ORGANIZATION REPORT NUMBER

9. SPONSORING / MONITORING AGENCY NAME(S) AND ADDRESS(ES)
Air Force Research Laboratory
29 Randolph Road
Hanscom AFB, MA 01731-3010

10. SPONSOR/MONITOR'S ACRONYM(S)
AFRL/RVBYE

11. SPONSOR/MONITOR'S REPORT NUMBER(S)
AFRL-RV-HA-TR-2008-1079

12. DISTRIBUTION / AVAILABILITY STATEMENT
Approved for Public Release; Distribution Unlimited.

13. SUPPLEMENTARY NOTES
Reprinted from: Proceedings of the 30th Monitoring Research Review – Ground-Based Nuclear Explosion Monitoring Technologies, 23 – 25 September 2008, Portsmouth, VA, Volume I pp 30 - 39.

14. ABSTRACT

At far-regional and near-teleseismic distances the early body-wave coda contains information that is potentially useful to monitoring seismologists. However, waveforms from this distance range are typically under-utilized because of propagation complexities that cause significant difficulties in seismogram interpretation. For example, the first ~20 seconds of a far-regional seismogram often include multi-pathed arrivals caused by the interaction of the wavefield with upper mantle discontinuities at 220 km, 410 km and 660 km depth. Depth phases (e.g., *pP, pP410, sP, sP410*, etc.) also add complexity to the early part of the seismogram since they can constructively or destructively interfere with the primary phase arrivals. Array observations from earthquakes in central Asia regularly exhibit a variety of complex phase phenomena, such as back-azimuth anomalies, emergent or late-arriving first arrivals, large amplitude secondary arrivals, and interference phenomena between upper mantle arrivals and depth phases.

We have developed array-based methods to improve the characterization of primary and early coda phase arrivals observed at far-regional and near-teleseismic distances. These techniques include improved signal processing to accurately measure the delay times (τ's) and slownesses (p's) of primary and secondary phases from small-aperture arrays. We use these τ–p measurements to develop representative crust and mantle velocity-depth profiles and suites of synthetic seismograms through those models. Then we use the processed array beams to derive 'wavefield templates'; i.e., grouped observations with similar phase characteristics. We analyze these wavefield templates by comparing them with synthetics, looking for quantitative explanations for the phase behaviors we observe.

Our approach results in a methodology that improves phase characterization and yields earth models that more accurately predict the succession of expected arrivals. We have applied our techniques to observations from two regional small-aperture arrays in Kazakhstan (MKAR and KKAR), and find that our results provide insight into wavefield behaviors that are regularly observed on the MKAR and KKAR arrays.

15. SUBJECT TERMS
Seismic characterization, Seismic propagation

16. SECURITY CLASSIFICATION OF:			17. LIMITATION OF ABSTRACT	18. NUMBER OF PAGES	19a. NAME OF RESPONSIBLE PERSON
a. REPORT	b. ABSTRACT	c. THIS PAGE			Robert J. Raistrick
UNCLAS	UNCLAS	UNCLAS	SAR	10	19b. TELEPHONE NUMBER *(include area code)* 781-377-3726

Standard Form 298 (Rev. 8-98)
Prescribed by ANSI Std. 239.18

IMPROVED PHASE CHARACTERIZATION OF FAR-REGIONAL BODY WAVE ARRIVALS IN CENTRAL ASIA

Aaron Ferris, Delaine Reiter, and Anastasia Stroujkova

Weston Geophysical Corp.

Sponsored by Air Force Research Laboratory

Contract No. FA8718-06-C-0002
Proposal No. BAA06-86

ABSTRACT

At far-regional and near-teleseismic distances the early body-wave coda contains information that is potentially useful to monitoring seismologists. However, waveforms from this distance range are typically under-utilized because of propagation complexities that cause significant difficulties in seismogram interpretation. For example, the first ~20 seconds of a far-regional seismogram often include multi-pathed arrivals caused by the interaction of the wavefield with upper mantle discontinuities at 220 km, 410 km and 660 km depth. Depth phases (e.g., *pP, pP410, sP, sP410*, etc.) also add complexity to the early part of the seismogram since they can constructively or destructively interfere with the primary phase arrivals. Array observations from earthquakes in central Asia regularly exhibit a variety of complex phase phenomena, such as back-azimuth anomalies, emergent or late-arriving first arrivals, large amplitude secondary arrivals, and interference phenomena between upper mantle arrivals and depth phases.

We have developed array-based methods to improve the characterization of primary and early coda phase arrivals observed at far-regional and near-teleseismic distances. These techniques include improved signal processing to accurately measure the delay times (τ's) and slownesses (p's) of primary and secondary phases from small-aperture arrays. We use these τ–p measurements to develop representative crust and mantle velocity-depth profiles and suites of synthetic seismograms through those models. Then we use the processed array beams to derive 'wavefield templates'; i.e., grouped observations with similar phase characteristics. We analyze these wavefield templates by comparing them with synthetics, looking for quantitative explanations for the phase behaviors we observe.

Our approach results in a methodology that improves phase characterization and yields earth models that more accurately predict the succession of expected arrivals. We have applied our techniques to observations from two regional small-aperture arrays in Kazakhstan (MKAR and KKAR), and find that our results provide insight into wavefield behaviors that are regularly observed on the MKAR and KKAR arrays.

OBJECTIVE

The objective of our research is to enhance the usefulness of regional, small-aperture arrays by developing array-based methods that can more accurately characterize far-regional (14°-29°) seismic wavefield structure. Far-regional (14°–29°) seismograms are particularly interesting because of the strong influence upper-mantle heterogeneity has on the early *P* coda arrival structure (< 20 secs). The suite of observed phases often includes multi-pathed arrivals and their depth phase counterparts, generated from wavefield interaction with upper mantle discontinuities at 220 km, 410 km, and a 660-km depth. The P-coda arrivals can be closely spaced in time (1–2 sec) and have similar ray parameters that range between 8–11 sec/degree. Further wavefield complexity arises from interference between depth-phase multiples and near-receiver scattered arrivals with the primary arrivals. These complexities can be region and earthquake specific.

The regional seismic arrays that have been built in the last fifteen years should be a rich data source for the study of far-regional phase behavior. The arrays are composed of high-quality borehole seismometers that make high-fidelity, low-noise recordings. However, beyond regional distances, the small apertures of these arrays (< 5km) limit their usefulness beyond first-arrival P- and S- onset picks. At these distances standard array methods (e.g., slant-stacking and frequency-wavenumber analysis) cannot resolve the arrival times and slownesses of primary and secondary arrivals, making the proper identification and classification of far-regional arrivals quite difficult. We are overcoming this limitation by applying refined array processing techniques in conjunction with straightforward wavefield generalization methodologies. Our goal is to characterize the commonly observed early coda arrivals that propagate from the different seismic regions of central Asia, utilizing recordings from the Makanchi (MKAR) and Karatau (KKAR) small-aperture arrays in Kazakhstan (Figure 1). This research will improve the usefulness of small-aperture arrays by increasing their ability to classify small-magnitude events that may be poorly recorded regionally and teleseismically.

RESEARCH ACCOMPLISHED

We have developed array-based methodologies to characterize the *P* coda of far-regional events using small aperture arrays. Our methodology includes several components: 1) improved small-aperture array processing to measure delay-times (τ) and slownesses (p) of primary and secondary arrivals; 2) construction of region-specific velocity-depth profiles derived from the τ-p measurements (i.e., τ-p transformations), as well as models derived from wavefield continuation methods, and 3) the derivation of 'wavefield templates' from clustering of array beams to capture the commonly observed arrival structure. These methods employ both theoretical and empirical techniques to reduce a large waveform data set (~600 earthquakes; Figure 1) into a smaller set of robustly observed wave phenomena. We then attempt to explain these phenomena using well-accepted, straightforward techniques. The separate components of our methodologies are discussed below.

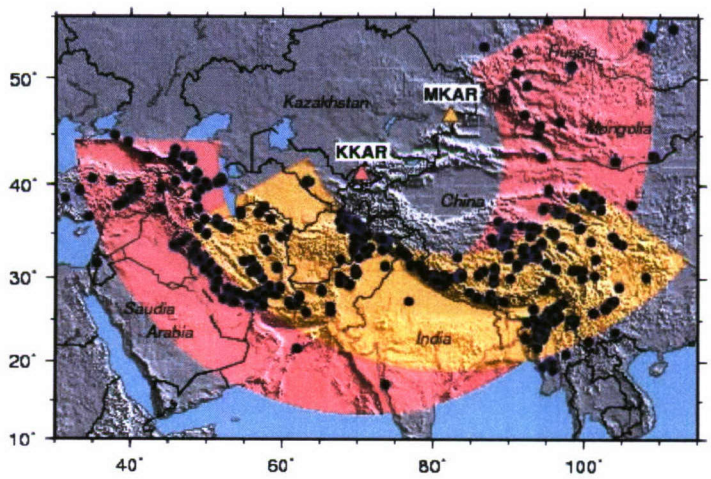

Figure 1. Map of central Asia showing the location of the Makanchi (MKAR) and Karatau (KKAR) arrays in Kazahkstan, as well as earthquakes (circles) used in this study. Colored bands mark the 14°–29° distance range from each array.

Improved Small-Aperture Array Processing

Our objective for the array processing is to compile a set a phase delay times (τ), slowness measurements (*p*) and array beams for our waveform data set of 600 central Asian earthquakes. The small aperture (< 5 km) of many of the newer arrays installed for nuclear monitoring purposes presents a serious challenge for typical array processing methods. However, we have developed and applied improved velocity spectra analysis (*vespa*) and phase-weighted stacking methods (PWS; Schimmel and Paulssen, 1997) to improve phase identification at small-aperture regional arrays. Our results indicate that in many cases we can detect closely-spaced arrivals by their slowness values in a time window that includes the direct *P* arrival, depth phases and arrivals from upper-mantle discontinuities (Ferris and Reiter, 2007).

In Figure 2 we show an example of applying phase-weighted stacking to a typical regional event recorded by the MKAR array. At a distance of 14.33° and depth of 17 km, a series of arrivals are predicted to occur within the first 16 seconds of this seismogram. In addition to the main *P* branch, the reference model iasp91 (Kennett and Engdahl, 1991) predicts the *pP* and *sP* depth phases at a delay time of ~4 seconds and ~7 seconds, respectively, relative to the first arrival. These depth phases are followed by their multi-pathed counterparts that bottom at the 410 km discontinuity and have a delay time of ~12 and ~14 seconds for *pP410* and *sP410*. When compared to the decomposed wavefield (represented by the phase coherence vespagram in Figure 2), it is not clear how these predicted arrivals correspond to the observations. Even the main *P410* arrival, which should be near the caustic of the travel-time branch and thus amplified, is not obviously identifiable. However, there may be interference between the *P410* and *sP* phase, as they are predicted to arrive within 0.3 seconds of each other. If the earthquake depth is decreased to 10 km, the *pP* and *sP* arrivals agree better with the observations. However, a change in focal depth does not account for all the observed arrivals, especially the coherent later arrivals near 15 seconds, or explain the ambiguity in the *P410* arrival.

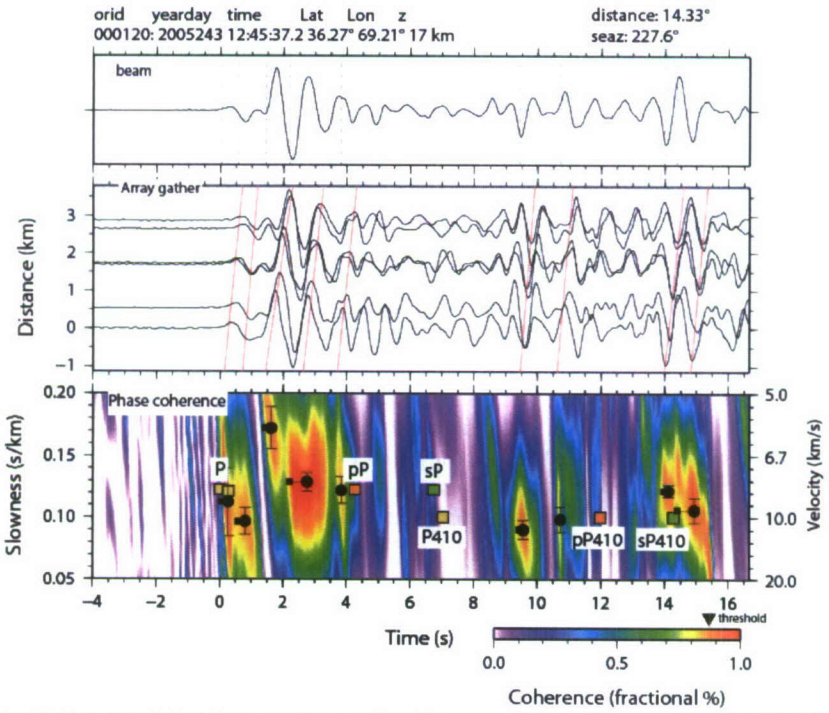

Figure 2. Example of phase-weighted array processing for an earthquake recorded by the MKAR array at an epicentral distance of 14.3. The top panel shows the array beam, computed using the slowness of the first arrival. Dashed lines mark the computed onset times. The middle panel shows the array gather and move-out curves for detected arrivals. The bottom panel shows the phase-weighted coherence vespagram. Black circles mark arrivals with phase coherence greater than 85% (i.e., detections); black squares mark the computed onset time. Colored squares show the iasp91 predicted arrivals (yellow = *P* branch , orange = *pP* depth phases, green = *sP* depth phases).

This exercise of comparing our array measurements to those predicted from global reference models illustrates the need for more region-specific models. The next component of our improved phase characterization scheme is to use our array measurement and array beams to derive models that can more accurately match the observations. Our methodologies to accomplish this and preliminary results are discussed in the following sections.

Regional Velocity Depth Profiles

To address the need for more applicable earth models and to generalize our array observations, we are developing two separate methods to derive velocity-depth profiles for the specific regions monitored by the MKAR and KKAR arrays. Both methods are based on τ-p (i.e., delay-time/slowness) techniques that decompose wavefields into their components parts. The first method involves directly inverting array-based delay-time and slowness measurements to solve for a velocity-depth function (e.g., Carbonell and Smithson, 1994). The second method applies wavefield continuation techniques to array-beam record sections to accomplish the same goal (e.g., McMechan, 1984). While these methods are not new, they are not typically applied to small-aperture array data, but rather to data from long linear arrays of seismometers (e.g., Morozov et al., 2005). Since we apply these methods to multiple events records, a main challenge is accounting for the effects of differing source parameters (origin time, event depth, and focal mechanism), which may be unknown or poorly constrained. While our methods are under active development, preliminary results show that we are able to extract reasonable models for specific regions in our study area. The two methods, direct inversion and wavefield continuation, are discussed below.

Direct Inversion of Array-Based Delay-Time and Slowness Measurements

Figure 3 illustrates how we prepare array-based delay-time and slowness measurements for velocity-depth inversion. In this example we groom the outliers from data set of measurements made at MKAR, consisting of 110 earthquakes ranging from 14°–29° epicentral distance, which includes earthquakes extending from the Hindu Kush region of Pakistan/Afghanistan to the Makran coast and Zagros Mountains of Iran. The grooming removes everything outside the 8.0–14.5 (sec/deg) slowness range, to help eliminate measurements from P-to-S scattered signals and coherent noise. We also discard measurements that exhibit significant slowness smearing (i.e., measurement uncertainties) during the PWS processing. Once the groomed measurements (Figure 3a) have been collected, we reduce them to a single τ-p curve by computing the error-weighted-mean τ value within evenly spaced slowness bins (Figure 3b), excluding bins with only a few measurements. Averaging the τ's within a common slowness bin acts to correct for errors in focal depth by accounting for the $\pm\tau$ offset between P and pP. While this is not a perfect correction due to missed phases in the array processing, the inclusion of sP arrivals, and measurement error, we have found it more effective and feasible than correcting τ on an event basis using catalog depths, which typically have large uncertainties. The averaged τ-p curves are the observations that are input into the velocity-depth inversions. The curve shown in Figure 3b generally agrees with the iasp91 τ-p curve; however, it is not as smooth, which may be partially caused by measurement error and inadequate averaging, not just differing earth structure.

Figure 4 shows a preliminary velocity profile determined from the MKAR τ-p data shown in Figure 3. There are many ways to parameterize this inverse problem, and the results in Figure 4 represent one solution. To derive the model we solved for the thicknesses of a sequence of layers that best fit the τ-p observations, using a damped least-squares formulation. For this particular inversion, we linearized the problem by assigning each slowness p to the layer representing its maximum depth of penetration (i.e., the ray turning point), which depends on the initial velocity-depth profile and is updated after each inversion iteration. The under-determined system of equations we invert is $\tau = G \cdot h$, where τ is a vector of our zero-offset time observations and h is vector of model layer thicknesses. Each row of G is composed of the vertical slowness through each layer up to the turning depth for each p observation. While linearizing the inversion allows a direct estimation of model uncertainties, the final results tend to be strongly influenced by the initial model. We are currently examining other algorithms to better understand model non-uniqueness, as well as other parameterizations of the linear inverse problem.

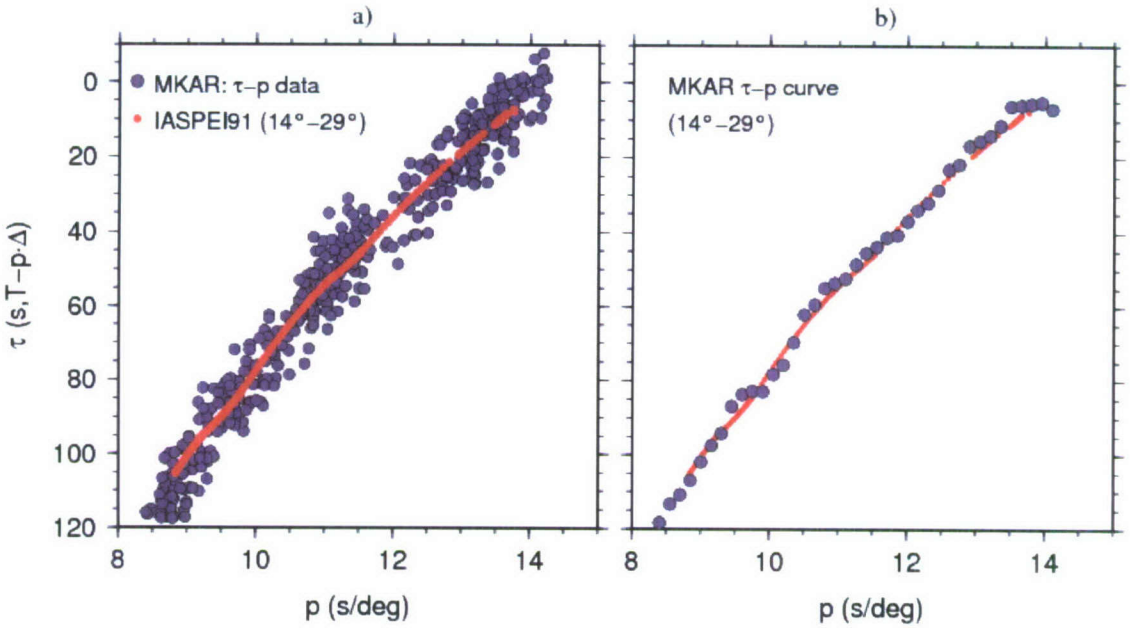

Figure 3. Sample τ-p data from the MKAR array. a) The groomed MKAR data (blue circles); red dots show the iasp91 τ-p curve for a surface-focus source. The range in τ for a particular slowness is caused by the difference in τ for earthquakes at different depths, rather than just measurement error. b) The averaged τ-p curve from the groomed data, evenly sampled in slowness at 0.15 sec/deg.

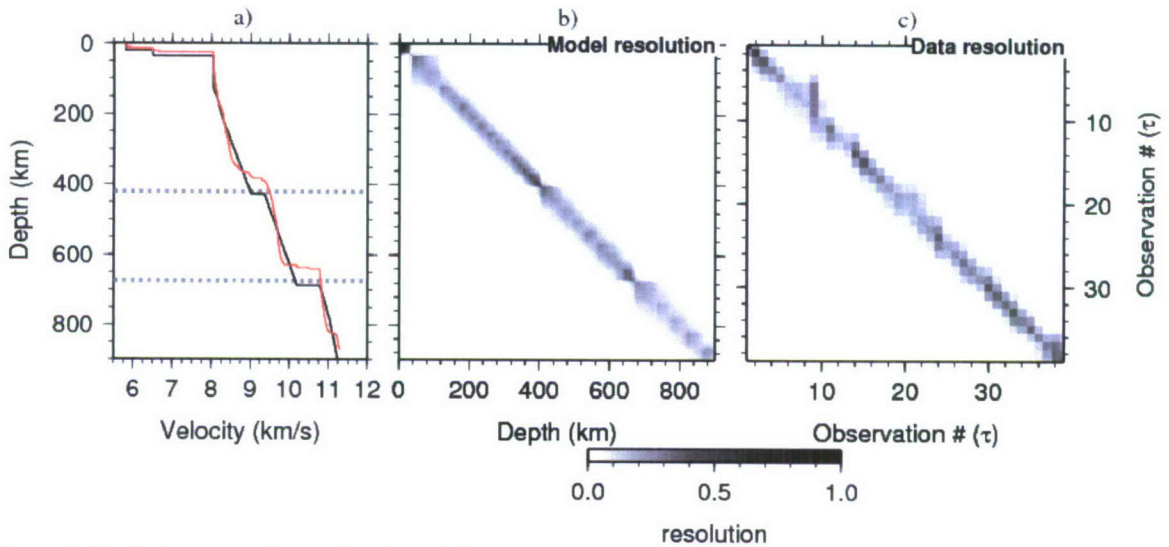

Figure 4. Preliminary τ-p inversion for a 1-D velocity profile of the MKAR data shown in Figure 3. a) final model (red) compared to the starting model (black); b) the model resolution matrix; and c) the data resolution matrix.

Wavefield Continuation Analysis using Array Beams

Wavefield continuation (e.g., Clayton and McMechan, 1981) is commonly used to extract velocity profiles from record sections recorded by long linear arrays of sensors. In our case, array beams form the record sections. We

arrange the beams according to their epicentral distance and align them based on the first arrivals (Figure 5a). Arrivals are aligned relative to a reference model, a time shift that acts as an event-based static correction. The correction tries to account for the differences in earthquake depth and origin time. This is a simplistic correction and does not correctly account for the time shifts of secondary phases (i.e., pre-critical arrivals from the major discontinuities), whose arrival times relative to the first arrival depend on earthquake depth. However, some type of correction needs to be made to each array beam in order to get a reasonable τ-p transformation. To account for the difference in source mechanism, we perform the wavefield continuation calculations on the envelopes of the beams rather than the raw amplitude records. This acts as a low-pass filter, reducing the resolution of the resulting velocity-depth profile.

The wavefield continuation method consists of two linear transformations of the wavefield record sections. First, record sections are slant stacked, transforming them from the distance-time domain into the τ-p domain (Figure 5b). This is followed by a downward continuation, or depth migration, of the wavefield to transform the τ-p data to the slowness-depth plane. This second step is an iterative process, where the τ-p data are repeatedly migrated until the slowness-depth image converges to the input velocity model (Figure 5c). There are several ways to update the velocity model between iterations. We are currently using a scheme that picks the maximum amplitude at each depth from the slowness-depth image and then computes the weighted average between it in the input velocity model. This scheme performs adequately; however, noise in the initial τ-p transformation can cause artifacts in the final velocity-depth profile. We are currently working on methods to improve the iterative migration procedure.

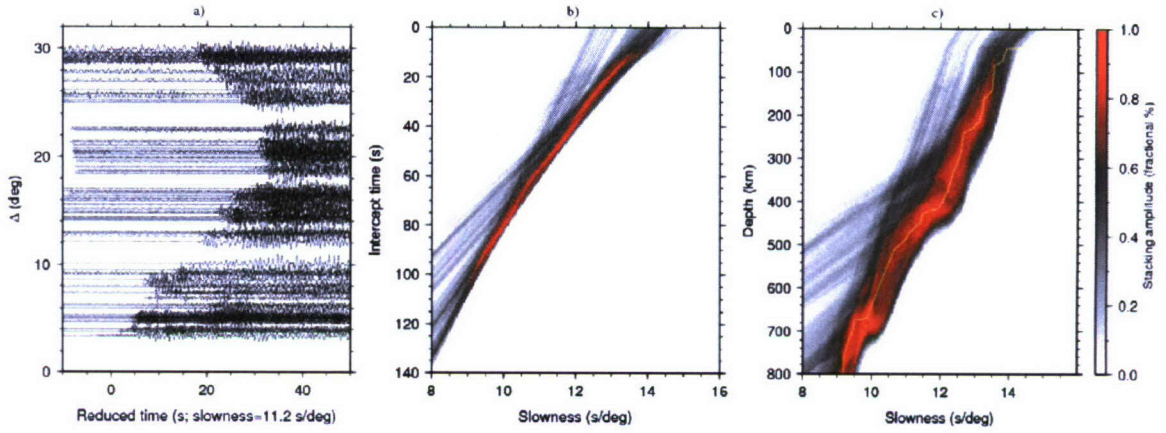

Figure 5. Example showing the transformation of a record section (a) to the τ-p domain (b) and the downward continuation to the slowness-depth domain (c). Array beams are from 104 earthquakes that extend from the Hindu Kush region of Pakistan/Afghanistan to the Makran coast and Zagros mountains of Iran.

Figure 6 shows a comparison of our preliminary velocity-depth profile derived from the wavefield continuation procedure to the iasp91 model. Below 400 km depth, our model exhibits moderately slower velocities than iasp91, and a gradient zone at the 410 km rather than a sharp discontinuity (Figure 6a). A comparison of the slowness vs. distance curves for the predicted P arrivals for each model are shown in Figure 6b. Here the differences are more apparent, where our derived model shows more structure above the 410 km discontinuity (slowness < ~12 sec/deg), and a significant difference in the caustic points of both the 410 km (termination of B-C branch in Figure 6b) and 660 km discontinuity (termination of D-E branch). While our model is preliminary, some of the features we observe may be related to an inadequate distance sampling of our array beams, as well as the windowing procedure used in the initial τ-p transformation. Both of these would explain the initial appearance of the predicted 410 km and 660 km triplicate arrivals at greater distances (18° and 20°, respectively) in our derived model than the iasp91 model, where they appear at 14° and 18°, respectively.

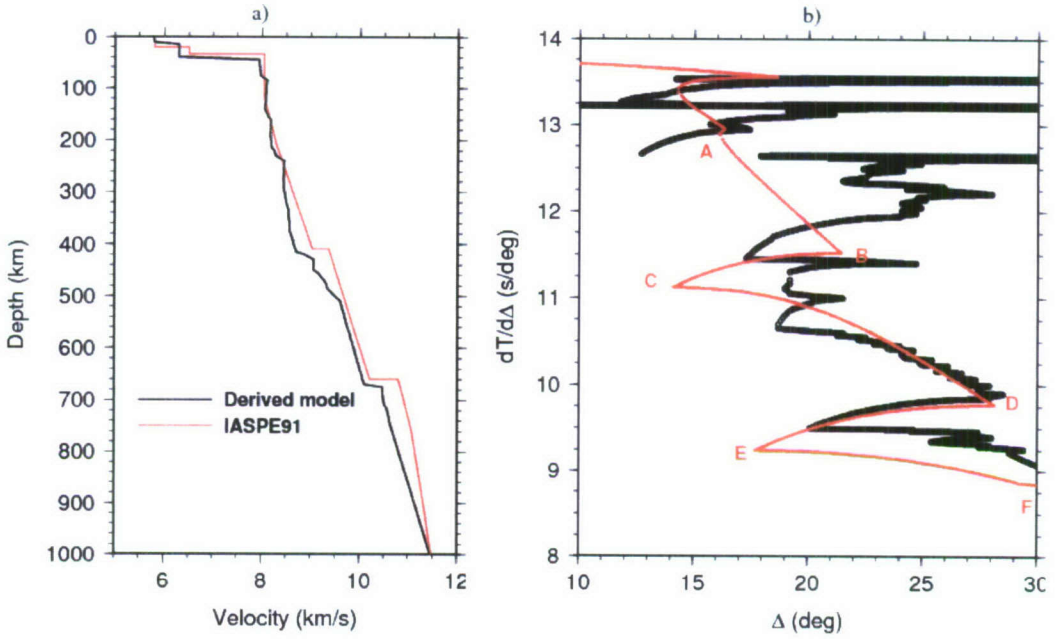

Figure 6. Comparison of the velocity-depth profile from wavefield continuation to the iasp91 reference model: (a) derived model (black) and iasp91 model (red). (b) Slowness vs. distance comparison between the derived model (black) and the iasp91 model (red) for predicted *P* arrivals.

Waveform Templating for Groups of Like Waveforms

Another component of our phase characterization methodology is the analysis of the array beams using clustering techniques. In addition to the arrival times and slowness of the coda phase arrivals, phase-weighted stacking analysis yields array beams, which are then input to a waveform clustering algorithm. The algorithm is based on 'fuzzy clustering' to form groups of beams that exhibit similar characteristics; it has been used widely in pattern recognition applications (Bezdek, 1981). Clusters are defined by assigning each beam a cluster membership value, which is a quantitative measure that incorporates a distance measure between each array beam and a representation of the cluster centers. We have experimented with distance measures involving *L1* and *L2* norms, as well as waveform semblance, with varying degrees of success that depend on data noise levels. From each cluster of similar beams, we derive a template waveform using a stacking process that weights each cluster member by its degree of membership to that particular cluster. The 'fuzziness' of the method allows a single beam to be a member of more than one cluster group. The objective behind the waveform clustering is to reduce the database of observations to a set of representative waveforms that exhibit consistent phase-arrival behavior. Sometimes the clustering is geographic, but there are other wave phenomena that can also produce groupings of similar waveforms

Figure 7a shows the cluster group and its associated wavefield template that results from applying our waveform clustering algorithm to the set of 100 events shown in Figure 7b. These beams are derived from seismograms recorded by the MKAR array in the 14°–29° distance range that extends from northern Pakistan to the Makran coast in Iran. In this example, the algorithm clusters the events into 5 groups, with 12–24 members per group. We applied an *L2*-norm distance measure and aligned the array beams prior to clustering using multi-channel cross correlation (VanDecar and Crosson, 1990), applied to the first four seconds of each beam signal. We have found the alignment of the beams to be beneficial to the clustering procedure. However, the length of the cross-correlation window is an important variable. For example, if the window is too long, the array beams align on the maximum amplitude signal in the record. For some beams, the maximum amplitude arrival may occur early in the seismogram, while for others it occurs much later. This can result in some unusual clustering of events that seems counter-intuitive. For this reason, we find clustering methods based strictly on cross correlation, as used in other types of studies (e.g., Menke 1999; Ferretti et al., 2005; Barani et al., 2007) are not suitable for our particular needs.

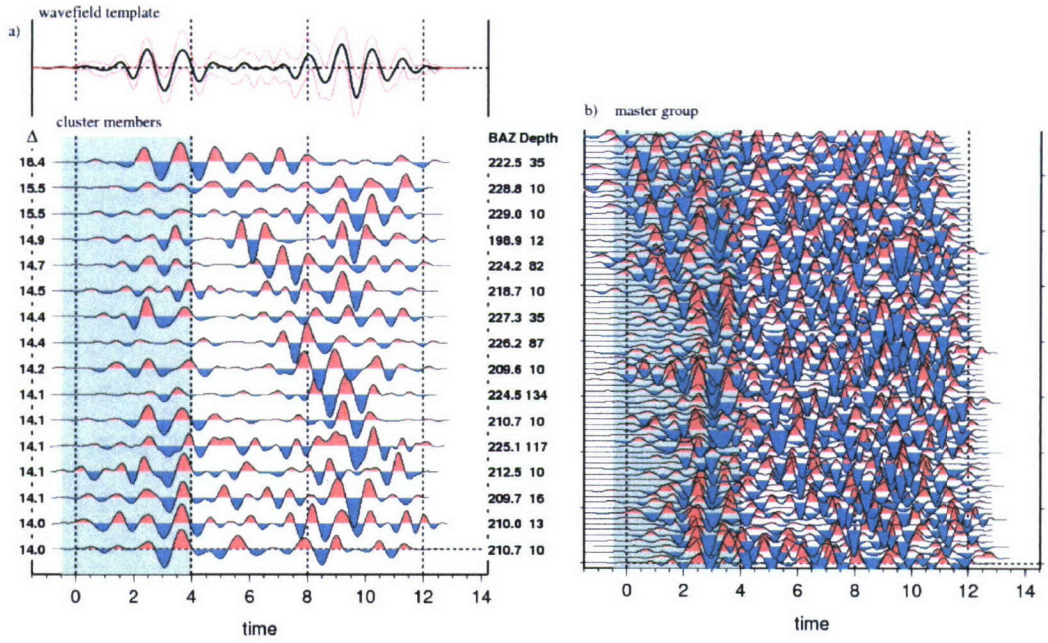

Figure 7. Example of wavefield clustering to generate a wavefield template. (a) The bottom panel shows the cluster members sorted by epicentral distance (shown on the left). The green band highlights the time band of cross correlation. The top panel shows the computed wavefield template (black) and 1-σ deviation (red). (b) A record section of all 100 earthquakes input to the clustering algorithm.

For the example shown in Figure 7, the resulting cluster members include earthquakes that are near the 14.3° distance range, but some more distant earthquakes are also included. The earthquake depth range is also variable, but may be due to poorly constrained catalog depths. In general, the cluster members show consistent waveform structure in the cross-correlated portion of the signal. Later arrivals show more variability between the cluster members, but still appear to align well at approximately 8 seconds and later. The most variability occurs between 4 and 8 seconds delay time, where some records show large amplitude arrivals while other show little signal. Some of this variability is likely due to differences in earthquake distance, triplicated arrivals, and the presence of depth phases. We continue to refine and improve the wavefield clustering algorithm.

Phase Characterization Analysis

To characterize observed phase arrivals, we calculate different misfit measures between our suite of body-wave synthetic seismograms and the observed wavefield templates. Since the synthetic waveforms are generated from models derived from the τ-p data, arrival times of the wavefield templates should be well matched. We note that to derive meaningful measurements, we must account for frequency content and amplitude variations.

Figure 8 provides an example of how we fit the synthetic seismograms to the wavefield template shown at the right of Figure 7. We computed synthetics using a test model (CRUST2.0 over AK135) for focal depths ranging from 0–60 km and event distances between 14° and 30°. Then we calculated the *L2* root-mean-square (RMS) residual of the differences between the wavefield template and each synthetic seismogram. The left panel in Figure 8 shows the results of this exercise, with a black cross denoting the distance (15.4°) and depth (32 km) at which the minimum RMS value occurs. In general, the best-fitting synthetic fits the overall structure of the template, even though the method is fairly crude. However, a portion of the wavefield template does not fit well (between 7–8 s), and this may be due to a number of causes. For instance, the test model we used to generate the synthetics may be inaccurate. Also, the focal mechanism or the misfit measure we employed in the comparisons could be inadequate.

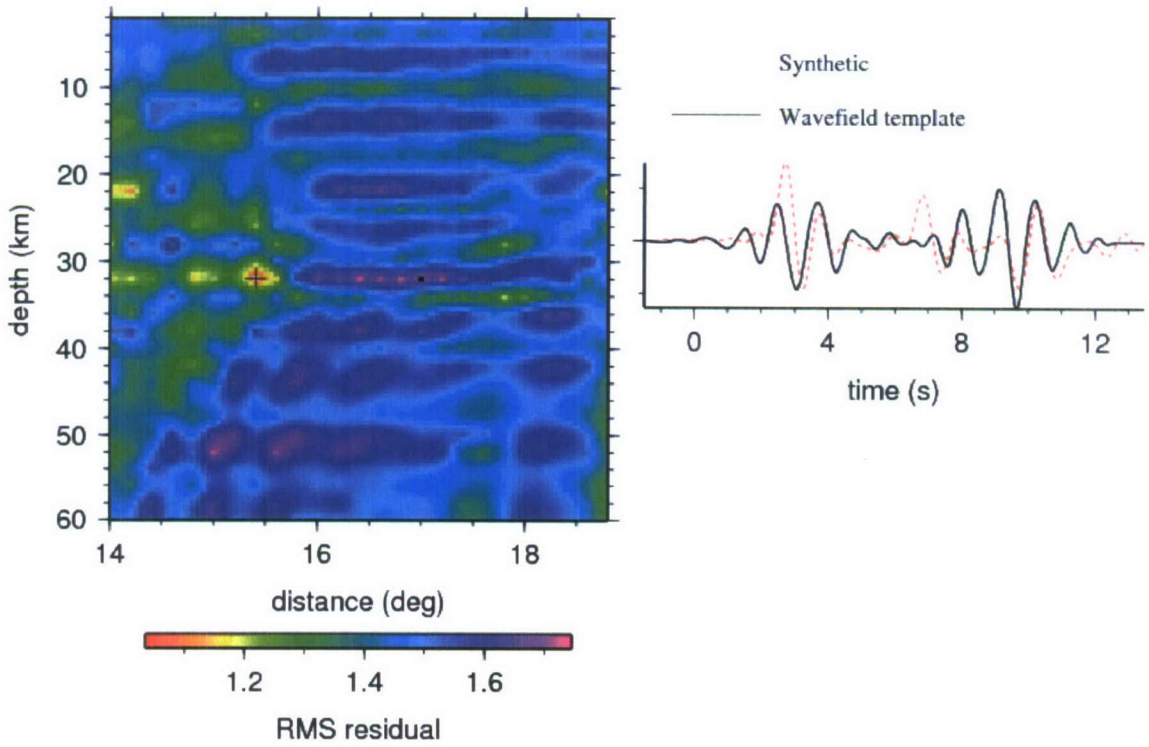

Figure 8. Example of fitting synthetic seismograms to an empirical wavefield template. Right panel shows the wavefield template (black) and the best-fitting synthetic (red). The left panel shows an image of the root mean-square residual between the wavefield template and a suite of synthetics computed for varying event distance and depth. The best-fitting synthetic for this wavefield template corresponds to a distance of 15.4° and an event depth of 32 km (black cross).

CONCLUSIONS AND RECOMMENDATIONS

Regional seismic arrays that have been recently installed for nuclear monitoring are under-utilized in the study of far-regional arrivals. The small aperture of many of these arrays (< 5km) restricts their usefulness at these distances beyond first arrival onset picks of *P* and *S* waves. However, our research is overcoming this limitation by applying refined array processing techniques in conjunction with τ-*p* and wavefield templating analysis methods. Our methodology improves the characterization of primary and early coda-phase arrivals observed at far-regional and near-teleseismic distances. Our approach is to distill the wide variety of seismicity we observe to subsets of commonly and robustly observed phase-arrival phenomena. We are then using well-accepted modeling and inversion techniques to explain these phenomena. Our aim is to explain as much of the phenomena as we can with simple and straightforward techniques, leaving the anomalies for future research.

We are developing and applying our techniques to central Asian earthquakes recorded on the MKAR and KKAR arrays in Kazahkstan. Our results indicate that we can differentiate between the numerous arrivals of the early coda. However, global reference models cannot capture the phase succession and arrival-time behavior we observed from the complex tectonic regions of central Asia. To address this, we are developing regional 1-D models directly from the array measurements (delay-times, slowness, and beams). Since these models are derived from the data, they should better explain the phase behavior we observe from specific regions. To test these models and further improve phase characterization, we are constructing 'wavefield templates' through cluster analysis to generalize the waveform structure from the different seismic regions. The templates are then used in a waveform fitting analysis to gain a better understanding of the phase phenomenon observed from the complex seismic regions of central Asia.

REFERENCES

Barani, S., G. Ferretti, M. Massa, and D. Spallarossa (2007). The waveform similarity approach to identify dependent events in instrumental seismic catalogues. *Geophs. J. Int.* 168: 100–108.

Bezdek, J. C. (1981). Pattern recognition with fuzzy objective function algorithms, Plenum Press, New York.

Carbonell, R. and S. B. Smithson (1994). Inversion of reflected *PP*, *SS*, and converted *PS*/*PP* travel times for crustal structure, *Bull. Seism. Soc. Am.,* 84, 1889–1902.

Clayton, R. and G. McMechan (1981). Inversion of refraction data by downward continuation, *Geophysics* 46: 6, 860–868.

Ferretti, G., M. Massa, and S. Solarino (2005). An improved method for the recognition of seismic families: Application to the Garfagnana-Lunigiana Area, Italy. *Bull. Seism. Soc. Am.* 95: 1903–1915.

Ferris, A. and D. Reiter, (2007). Using small-aperture arrays to identify far-regional P-wave arrivals, in *Proceedings of the 29th Monitoring Research Review: Ground-Based Nuclear Explosion Monitoring Technologies*, LA-UR-07-5613, Vol. 1, pp. 14–23.

Kennett B. L. N. and E. R. Engdahl (1991). Travel times for global earthquake location and phase identification, *Geophys. J. Int.* 105: 429–465.

McMechan, G. A. (1984). Inversion of a refraction wavefield by imaging in the p-x and v-z planes, *Geophys. J. R. Astr. Soc.* 78: 723–733.

Menke, W. (1999). Using waveform similarity to constrain earthquake location, Bull. *Seism. Soc. Am.*, 89, No. 4, 1141–1146.

Morozov, I. B., E. A. Morozova, S. B. Smithson, P. G. Richards, V. I. Khalturin, and L. N. Solodilov (2005). 3D First-arrival regional calibration model of northern Eurasia, *Bull. Seism. Soc. Am.* 95: 951–964.

Schimmel N. and H Paulssen (1997). Noise reduction and detection of weak, coherent signals through phase weighted stacking, *Geophys. J. Int.* 130: 497–505.

VanDecar, J. C., and R. S. Crosson (1990). Determination of teleseismic relative phase arrival times using multi-channel cross-correlation and least squares, *Bull. Seis. Soc. Am.* 80: 1, 150–159.